Mathematical Biosciences and Engineering

http://www.aimspress.com/journal/mbe

MBE, 23(6): 1687–1707.
DOI: 10.3934/mbe.2026061
Received: 21 January 2026
Revised: 01 April 2026
Accepted: 16 April 2026
Published: 14 May 2026

Research article

Exploring the effect of density dependent infection rate in a within host viral infection model

Hope Sage and Hana M. Dobrovolny*

Department of Physics & Astronomy, Texas Christian University, 2800 S. University Drive, Fort Worth, TX 76109, USA

* **Correspondence:** Email: h.dobrovolny@tcu.edu.

Abstract: The most common viral dynamics models for analyzing viral infections assume a well-mixed spatial distribution between viral particles and uninfected target cells. However, throughout an infection, the spatial distribution of virus and cells changes. Initially, virus and infected cells are localized so that a target cell in an area with lower virus presence will be less likely to be infected than a cell close to a location of viral production. A density-dependent infection rate has the potential to improve models that treat the cellular infection probability as a constant. Building on previous work that used epidemiological models, which introduced Saturated Incidence, Beddington-DeAngelis, and Crowley Martin models to simulate spatial heterogeneity in population-level models, we implemented these density-dependent models in within-host viral kinetics models to understand how a density dependent infection rate might impact the predicted severity of an influenza infection. The parameter values that govern the strength of density dependence were varied to understand the implications of density dependent infection rate on disease severity and the potential impacts on patient treatment. For low density dependence, a steeper increase in the virus and a higher viral peak was predicted. We find that the initial localization of infected cells slows the progression of the infection, thus suggesting that accounting for density dependence when analyzing influenza infection severity can result in an altered expectation for viral progression.

Keywords: density dependence; heterogeneity; mathematical model; influenza; infection rate

1. Introduction

Influenza is a serious disease that affects many people worldwide every year with substantial illness and financial burden [1]. Each flu season, approximately 8 percent of the United States population suffers from the flu [2]. The total yearly economic impact of influenza on the US economy is upwards of 10 billion dollars [3]. Globally, influenza is estimated to account for 650,000 deaths annually [3].

Given the severity of medical and economic impacts from influenza, increasing our understanding of viral progression is essential in order to reduce the extent of symptoms associated with infection and to improve clinical outcomes.

Mathematical modeling provides a cost-effective approach to analyze, predict, and understand viral kinetics. Mathematical models have been developed to account for a wide range of viruses [4–8], and have been used to study antiviral drugs [9–11], the effect of the immune response [12, 13], and age differentiated outcomes [14, 15]. By employing mathematical models, clinicians and researchers can be better equipped to understand how untreated disease will progress, as well as provide a foundation to theoretically test treatment options before exploring more resource intensive actions including animal and human laboratory testing. Biophysical models contribute to an increased understanding of the progression of disease and can result in better estimations of predicted infection severity [16–18].

Work done by Baccam et al. laid a foundation for applying mathematical models to H1N1 influenza progression [4]. They used a system of four differential equations that accounts for changes in populations of uninfected target cells, cells in a noncontagious phase of intracellular viral replication, infectious cells, and virus. Through data fitting, accounting for an eclipse phase was found to provide an effective method to account for the delay between an uninfected cell's contact with virus and the time of release of the first virion [19, 20]. However, the model assumes equal spatial contact between all cell types and virus, which is inconsistent with biophysical understanding of viral progression. Early on in an infection, the virus is highly localized and does not have equal surface area contact with all uninfected cells [21–23].

A similar issue arises when modeling the spread of infectious diseases at the population level using compartmental susceptible-infected-recovered (SIR)-type models. In this case, the epidemic starts locally, with friends and family of the initially infected person being exposed, while the population at large is likely unaware that an infectious disease has taken root [24, 25]. Epidemiological models have dealt with this issue by introducing density-dependent transmission functions [26, 27]. Specifically, three models are commonly used to model density-dependent transmission: the saturated incidence model [28], the Crowley-Martin incidence model [29], and the Beddington-DeAngelis incidence model [30]. Mathematical analyses and simulations of these models shows that the choice of transmission function and the strength of the density-dependent parameters can determine whether an epidemic is initiated and how many people become infected [31–34].

At the within-host level, the use of density-dependent infection functions has not been fully examined, even though within host infections have similar spatial heterogeneity issues as the spread of infectious diseases at the population level. However, density-dependence has been incorporated into other steps of the viral replication process. One model modified the death rates of infected cells to account for changes in spatial distribution between uninfected cells, infected cells, eclipse cells, and virus [35]. Additionally, density-dependence has been used to model virus-mediated cell-cell fusion, with one study finding that a density-dependent fusion rate is needed to accurately capture fusion when the receptor density is low [36]. This study found that modifications to the syncytia formation rate were essential to accurately represent the experimental data. Finally, a within-host model used a Michaelis-Menton-like infection rate to account for the spatial distribution of semi-infectious particles [37]. The idea of density-dependent contact rates has been borrowed from epidemiological studies and is starting to be incorporated in some within host mathematical models [38–41], although the effect of this assumption has not been explored in isolation.

Here, we investigate three models of density-dependent infections to assess their impact on the time course of influenza infection. By varying density dependent constraints, we determined the impact of spatial heterogeneity on the infection severity and duration. Measurements of the viral titer curve and basic reproduction number of the system as a function of density dependent parameters show that increasing the density dependence tends to slow the progression of the infection, thus leading to a lower upslope, and a delayed and lower peak viral load.

2. Methods

2.1. Density dependent infection functions

The most common viral dynamics models for analyzing viral infections assume an even spatial distribution between the viral particles and the target cells. However, throughout an infection, the spatial distribution of the virus and cells changes. The standard influenza viral kinetics model first used by Baccam et al. [4],

$$\begin{aligned} \frac{dT}{dt} &= -\beta VT \\ \frac{dE}{dt} &= \beta VT - kE \\ \frac{dI}{dt} &= kE - \delta I \\ \frac{dV}{dt} &= pI - cV, \end{aligned} \tag{2.1}$$

assumes that a change in the uninfected target cells, T, is proportional to the interaction between uninfected target cells and viral particles with a constant infection rate β. Uninfected target cells that become infected enter an eclipse phase, E, where the virus replicates within the cell. Then, the cells become infectious, I, at a rate k. Once infectious, cells produce virus, V, at a rate p. All infectious cells are assumed to die after a time of $\frac{1}{\delta}$, while the virus is cleared at a rate of c.

In order to account for the density dependence, we examined three density dependent mathematical functions typically used in epidemiological or ecological models [42–44]. The models we considered were a Saturated Incidence function, the Beddington De-Angelis function, and the Crowley-Martin Incidence model. In all three cases, the infection rate, β, is modified by dividing by a function of virus, target cells, or both. Thus, when the amounts of virus or target cells are high, the infection rate is reduced. The saturated incidence function assumes that the infection rate is only modulated by the amount of virus,

$$\begin{aligned} \frac{dT}{dt} &= \frac{-\beta VT}{1+\alpha V} \\ \frac{dE}{dt} &= \frac{\beta VT}{1+\alpha V} - kE \\ \frac{dI}{dt} &= kE - \delta I \\ \frac{dV}{dt} &= pI - cV. \end{aligned} \tag{2.2}$$

Here, α determines the strength of the density-dependent effect — a higher value of α results in a larger reduction of the infection rate as the amount of the virus increases. The Beddington-DeAngelis model assumes that the infection rate is dependent on both the target cells and the virus in an additive manner,

$$\begin{aligned} \frac{dT}{dt} &= \frac{-\beta VT}{1+\gamma T+\alpha V} \\ \frac{dE}{dt} &= \frac{\beta VT}{1+\gamma T+\alpha V} - kE \\ \frac{dI}{dt} &= kE - \delta I \\ \frac{dV}{dt} &= pI - cV. \end{aligned} \tag{2.3}$$

In this case, both α and γ determine the strength of this effect, with α determining the influence of virus and γ giving the influence of target cells. The final model, Crowley-Martin, assumes that the infection rate is dependent on both the target cells and the virus, but in a multiplicative manner,

$$\begin{aligned} \frac{dT}{dt} &= \frac{-\beta VT}{(1+\gamma T)(1+\alpha V)} \\ \frac{dE}{dt} &= \frac{\beta VT}{(1+\gamma T)(1+\alpha V)} - kE \\ \frac{dI}{dt} &= kE - \delta I \\ \frac{dV}{dt} &= pI - cV. \end{aligned} \tag{2.4}$$

Here, α is associated with the strength of the density-dependent effect of the virus, while γ is associated with the strength of the density-dependent effect of the target cells.

2.2. Model parameters

The parameter values for the H1N1 flu virus, as determined by [4], were used (Table 1) for the simulations, and α and γ were varied across a range to see how density-dependent parameter variations affected several measures of viral severity. Systems of differential equations for each model were solved using `scipy.odeint` in Python. To explore the effect of density-dependence, α was varied from 10^{-4} to 10^{3}, while γ was varied from 10^{-15} to 10^{-7}. The ranges for α and γ were chosen based on the model's behavior more than any biological arguments. We were looking for a range where we see changes in the predicted behavior when the parameter values change. Smaller values of these parameters have little effect on the infection dynamics since the density dependence is small, while larger values of these parameters are in the region where infections are abrogated, so further increases have no effect. Note that the actual values of these parameters are dependent on the units of virus (α) or cells (γ), so it's difficult to specify any absolute values for these parameters that would be biologically reasonable. Note that α and γ are plotted on a logarithmic scale in all figures.

Table 1. Model parameters, taken from Baccam et al. [4], except α and γ.

Variable	Meaning	Value
β	Infection rate	3.2×10^{-5} $(\text{TCID}_{50}/\text{mL} \cdot \text{d})^{-1}$
p	Viral production rate	4.6×10^{-2} $\text{TCID}_{50}/\text{mL} \cdot \text{d}$
k	Transition time to infectious cell	4.0 /d
δ	Infected cell life span	5.2 /d
c	Viral clearance rate	5.2 /d
α	Viral density-dependence	10^{-4}–10^{3} $\text{TCID}_{50}/\text{mL}$
γ	Cell density-dependence	10^{-15}–10^{-7} cells
V_0	Initial viral titer	7.5×10^{-2} $\text{TCID}_{50}/\text{mL}$
T_0	Target cells	4×10^{8} cells

2.3. Calculations for measures of the curve

Several measures of the viral titer curve were calculated to characterize how the infection changes with changes in the density dependence (Figure 1). The viral peak was determined by locating the maximum value of the curve, which also gives us the time of peak. The slope of the viral titer curve was found using a linear least squares fit over the primary time points of ascent (upslope) or descent (downslope) of the viral titer curve. The duration of infection for each model was found by subtracting the final time point at which the virus was above a threshold of 10 TCID_{50}/ml from the time that the viral titer initially rose to the threshold value. The area under the curve (AUC) was found using 300 trapezoidal approximations and verified with Simpson's rule,

$$\text{AUC} = \frac{b-a}{2n}(V_0 + V_f + 2\sum(V_{1:n-1})),$$

where n is the number of steps used to simulate time - 1, b and a are the final and initial time values, respectively, and V represents the virus.

Some other characteristics were calculated from the modified systems of equations. The basic reproduction number, R_0, describes how many target cells one infected cell will infect. R_0 was calculated using the Next Generation Matrix method where each system of equations was split into two matrices that represent new infections and transitions [45]. The basic reproduction number is used to define a boundary between growth and decay of the viral load, where $R_0 > 1$ leads to an infection that will grow and $R_0 < 1$ leads to an infection that decays from its initial viral load. If an antiviral is applied to the system, the minimum antiviral efficacy needed to suppress the infection is given by $\varepsilon = 1 - \frac{1}{R_0}$ [46]. We calculate the minimum drug efficacy for all three models to examine the effect a density dependent infection rate might have on antiviral treatment. Additionally, whttps://www.cdc.gov/flu/season/2022-2023.htmle calculated the infecting time, t_{inf}, which is the time it takes for the virus to leave an infected cell and infect another cell. The infecting time is calculated following the procedure outlined in [47].

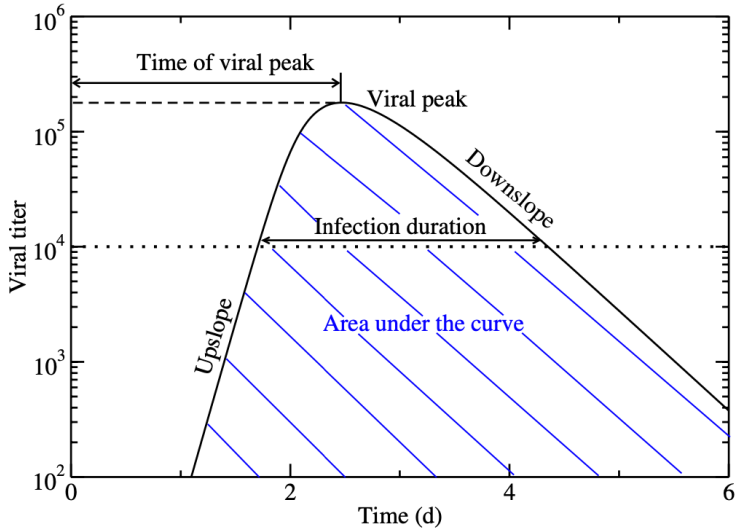

Figure 1. Measured aspects of the viral titer curve as related to changes in density dependence.

3. Results

Systems of differential equations that assume well-mixed spatial distributions were modified by varying parameters that constrain viral growth to understand how changes in spatial contact affect viral progression. Three different density dependent ordinary differential equation systems were used. Key aspects of the viral titer curve were measured to understand the possible outcomes of viral kinetics when density dependence is accounted for in models. The peak viral load, timing of the peak viral load, viral upslope, viral downslope, AUC, and infection duration were measured for ranges of α and γ.

3.1. Viral titer measurements

3.1.1. Saturated incidence model

Changes in the viral titer characteristics for the saturated incidence model are shown in Figure 2. As α increases, the viral maximum decreases, but the time to maximum increases before reaching a point where the density dependence is so high that the infection does not occur. The viral upslope generally decreases with a greater density dependence. At a higher density dependence, the downslope becomes rapidly less steep before leveling off towards zero. Initially, the infection duration increases quite rapidly. While our graph shows a plateau at 1000 days, this is due to the duration of our simulation — the infection duration will, in fact, continue to increase beyond 1000 days before it rapidly drops to zero for higher density dependent values. The AUC was lower for greater density dependence. The results suggest that the predicted measures of infection severity for a higher density dependence in the saturated incidence model result in a less severe infection with a lower maximum viral load and a slower viral growth compared to the model in [4].

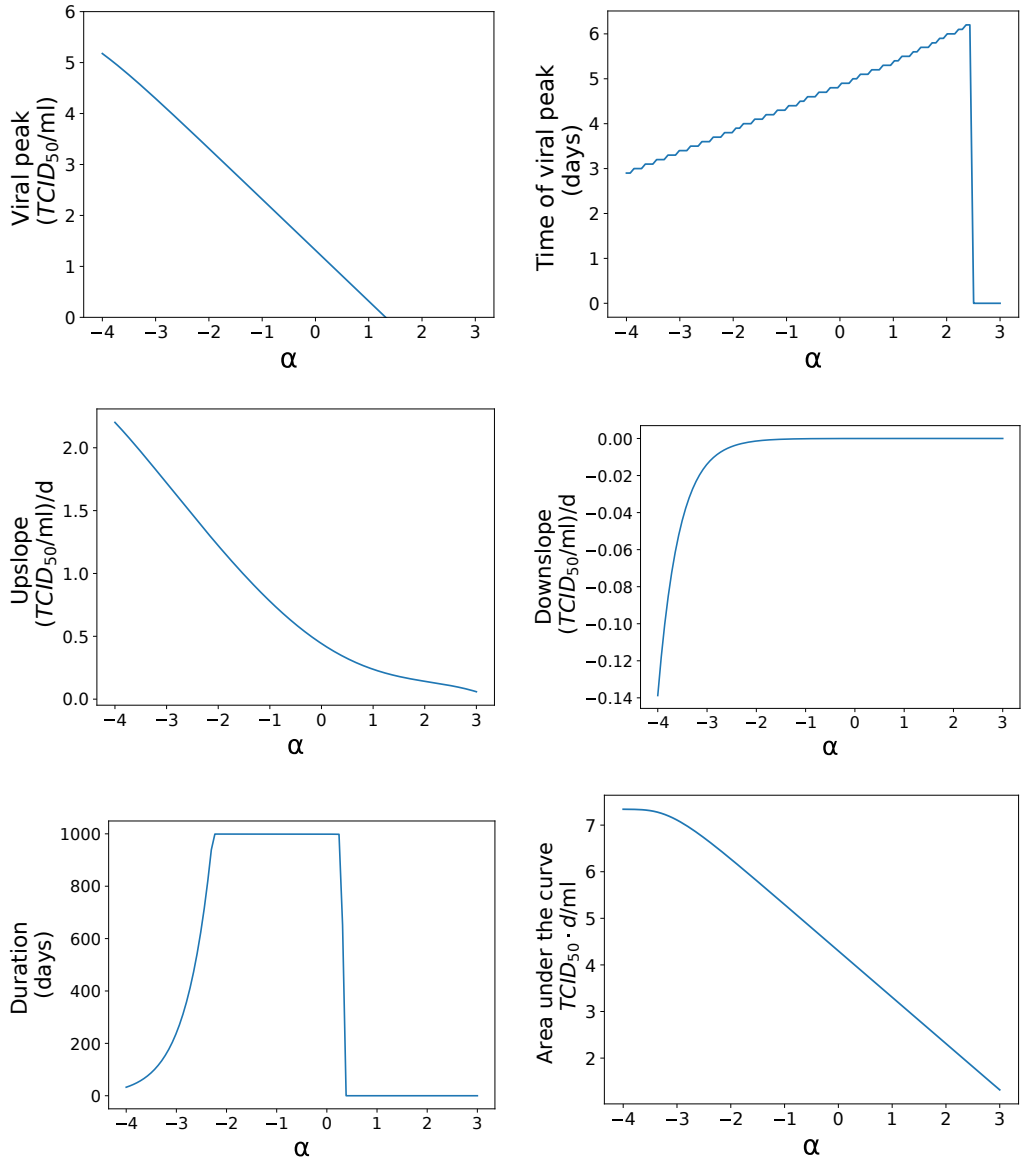

Figure 2. Measurements of the (top left) maximum viral load (log scaled), (top right) time of maximum, (center left) viral upslope, (center right) viral downslope, (bottom left) infection duration, and (bottom right) AUC (log scaled) of the Saturated Incidence Model when varying the parameter α. Note that α is plotted on a logarithmic scale.

3.1.2. Beddington DeAngelis model

Figure 3 shows predicted trends in the viral titer curve measurements based on variations in α and γ. For the Beddington DeAngelis model, the viral peak values are higher for a lower density dependence (low α and/or γ). The time of peak shows minimal variation related to the density dependence until a threshold α or γ value occurs that results in no infection. As a maximum γ value that allows for infection to occur is approached, a delay in the viral peak is observed. As α gets larger, there is not a similar delay in the time of viral peak. The predicted viral upslope is steeper for a lower density

dependence and decreases as both α and γ decrease, with a more gradual decrease as a function of α. The duration of infection becomes longer as α increases before falling to zero for higher α and γ values in an abrupt manner. The AUC is lower for greater density dependence values of α, with no infection occurring beyond a maximum value of γ. The Beddington DeAngelis model demonstrates that increases in the density dependence slow viral progression and decrease the maximum total amount of virus by limiting the ability of infection to spread.

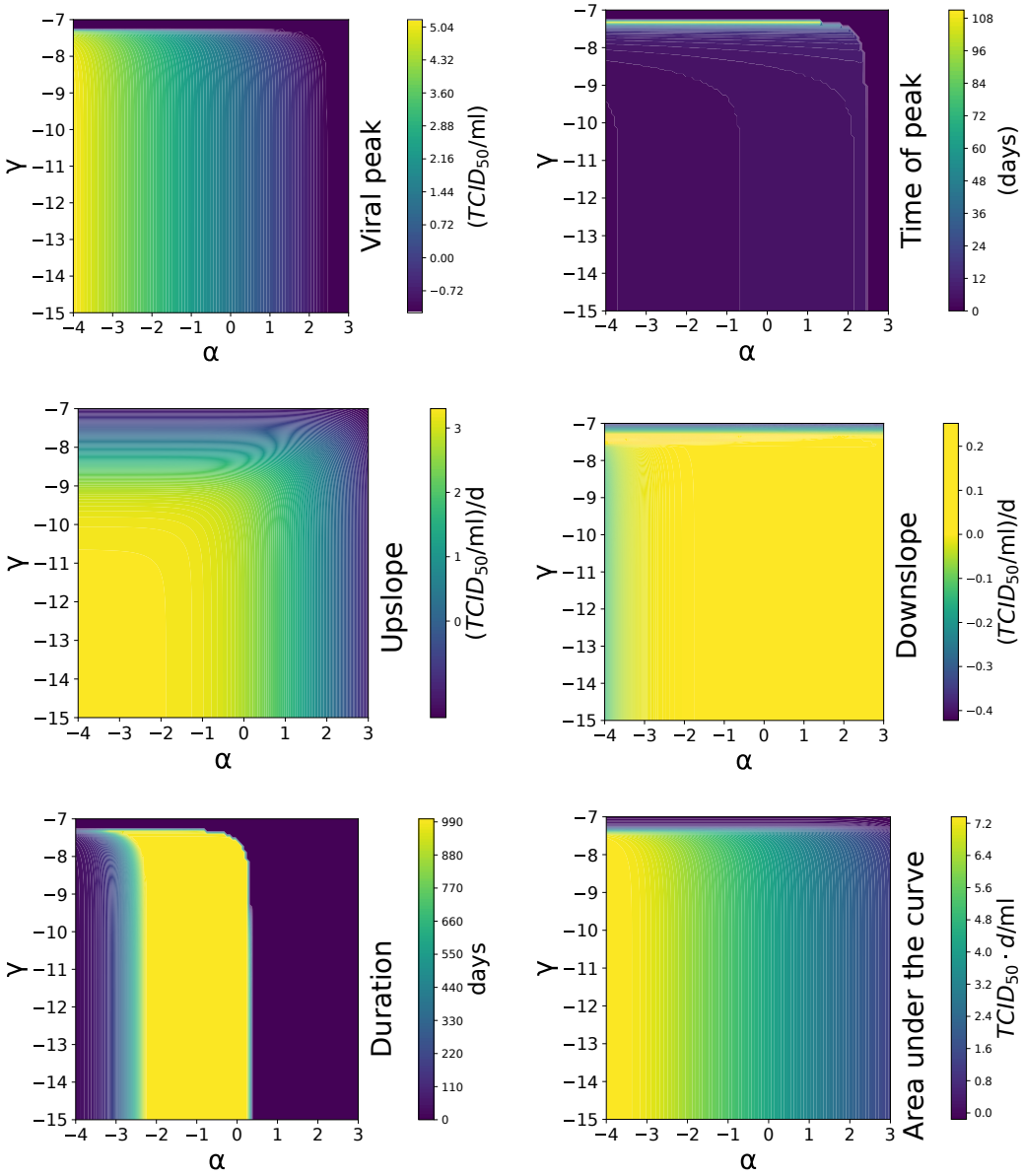

Figure 3. Heatmaps of the (top left) maximum viral load (log scaled), (top right) time at maximum, (center left) viral upslope, (center right) viral downslope, (bottom left) infection duration, and (bottom right) AUC (log scaled) of the Beddington DeAngelis model for varying density dependent parameters (α and γ). Note that α and γ are plotted on a logarithmic scale.

3.1.3. Crowley-Martin incidence function results

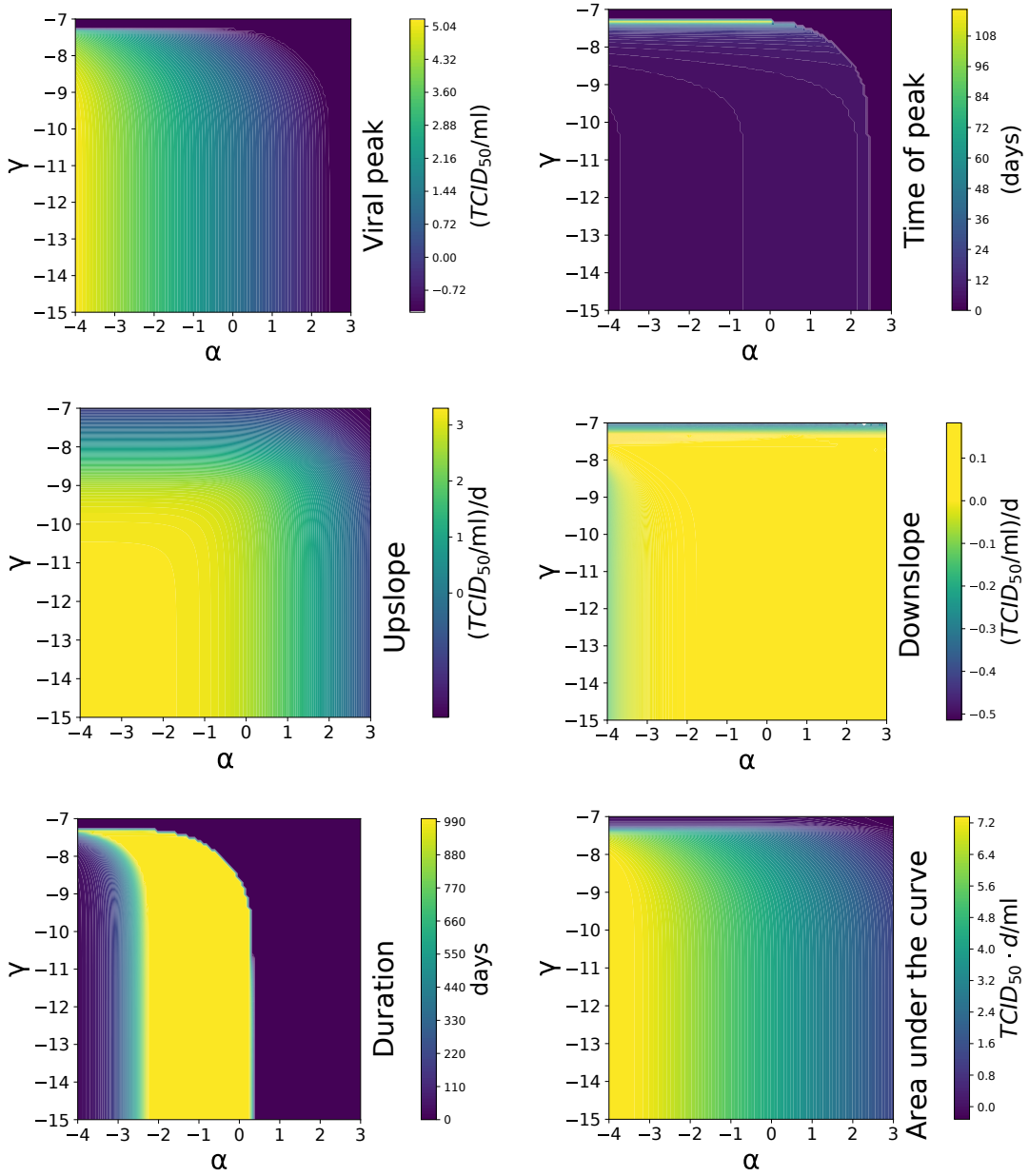

Figure 4. Heatmaps of the (top left) maximum viral load (log scaled), (top right) time at maximum, (center left) viral upslope, (center right) viral downslope, (bottom left) infection duration, and (bottom right) AUC (log scaled) of the Crowley Martin Incidence Model for varying density dependent parameters (α and γ). Note that α and γ are plotted on a logarithmic scale.

The Crowley-Martin Incidence function demonstrates similar predicted trends to the Beddington DeAngelis Model, as shown in Figure 4. For a lower density dependence, the viral peak is greater. The timing of the peak remains consistent despite varied density dependence values until reaching a

threshold value of α or γ where the infection no longer occurs. As this value is approached for γ, a delayed time to viral peak is briefly seen for higher γ values; however, this tendency is not observed as α values approach the boundary. For a lower density dependence, the viral upslope is greater, thus indicating a faster progression of infection. Very high levels of density dependence for γ lead to an increase in the downslope; however, the same is not observed for α. At high α and γ values, the predicted values for infection duration experience an abrupt drop to zero. This indicates that the infection duration remains fairly constant despite density variation until a point is reached where the virus cannot spread to produce an infection. The AUC is lower for greater density dependence values for α. For γ variation, changes in AUC were not observed until the γ values reached a threshold value That inhibited infection occurrence. These trends predict a less severe overall infection for a greater density dependence.

3.2. Basic reproduction number

The basic reproduction number, R_0, of the infection was calculated using the next generation matrix method and indicates the number of cells a single infectious cell will infect [48]. For R_0 values greater than one, the viral load will continue to increase and the infection will become more severe. For R_0 values below one, the viral load will decrease and the infection will regress. As a result, R_0 is crucial to understand how the infection will continue to develop and to develop effective treatment options.

The next generation matrix method splits each differential equation system into F and V matrices that represent new infections and transitions between or away from infected states. F and V matrices used in R_0 calculations are given in the supplementary material. R_0 is the largest eigenvalue of the next generation matrix. The basic reproduction numbers for the three models are as follows:

- Saturated Incidence:

$$R_0 = \frac{\beta p T_0}{(1 + \alpha V_0)^2 \delta c}.$$

- Beddington De-Angelis model:

$$R_0 = \frac{\beta p T_0 (1 + \gamma T_0)}{(1 + \gamma T_0 + \alpha V_0)^2 \delta c}.$$

- Crowley Martin model:

$$R_0 = \frac{\beta p T_0}{(1 + \gamma T_0)(1 + \alpha V_0)^2 \delta c}.$$

R_0 values are substantially lower for simulations with a greater density dependence (Figure 5). Lower R_0 values indicate a less extensive spread of virus within the body [49], which supports the idea of less contact between target cells and virions. As a result, spatially localized mixtures predict a less rapid progression of influenza than well-mixed particle distributions.

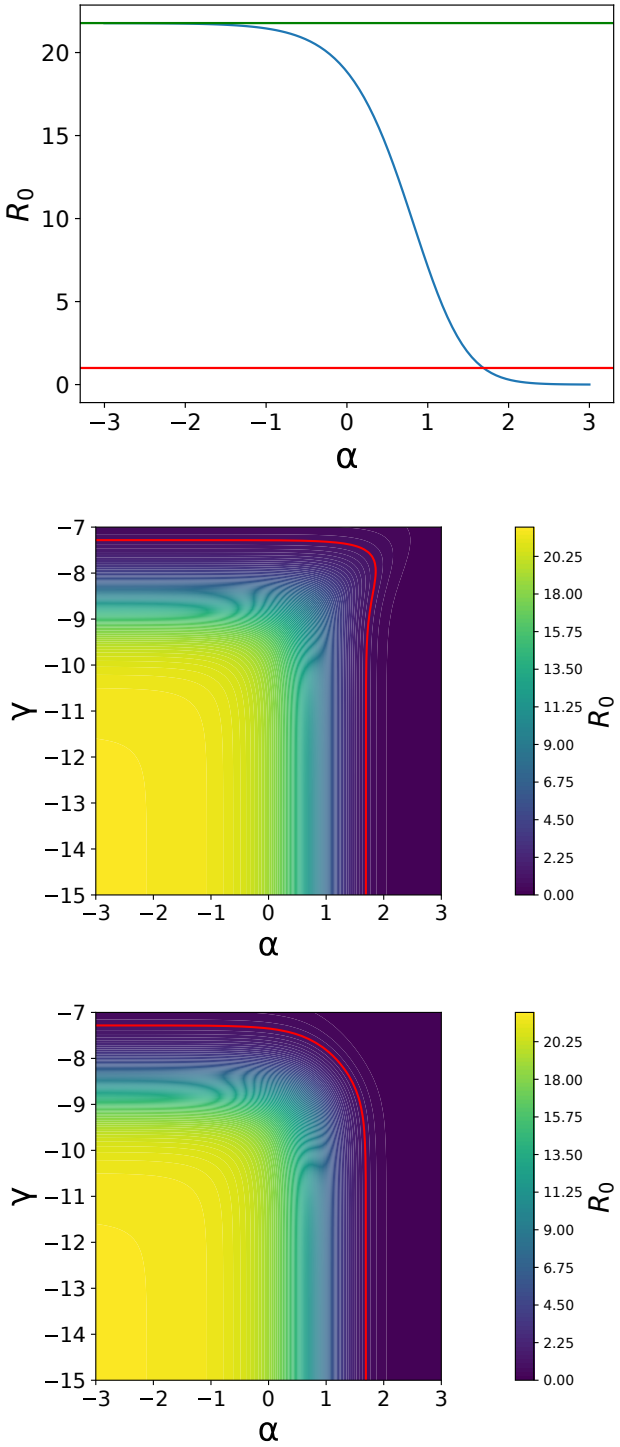

Figure 5. R_0 for different density-dependent models. (top) R_0 for the saturated incidence model, (middle) R_0 for the Bedington De-Angelis model, and (bottom) R_0 for the Crowley Martin model. $R_0 = 1$ is labeled in red and R_0 calculated from the model not accounting for density dependence is in green [4]. Note that α and γ are plotted on a logarithmic scale.

3.3. Drug efficacy measures

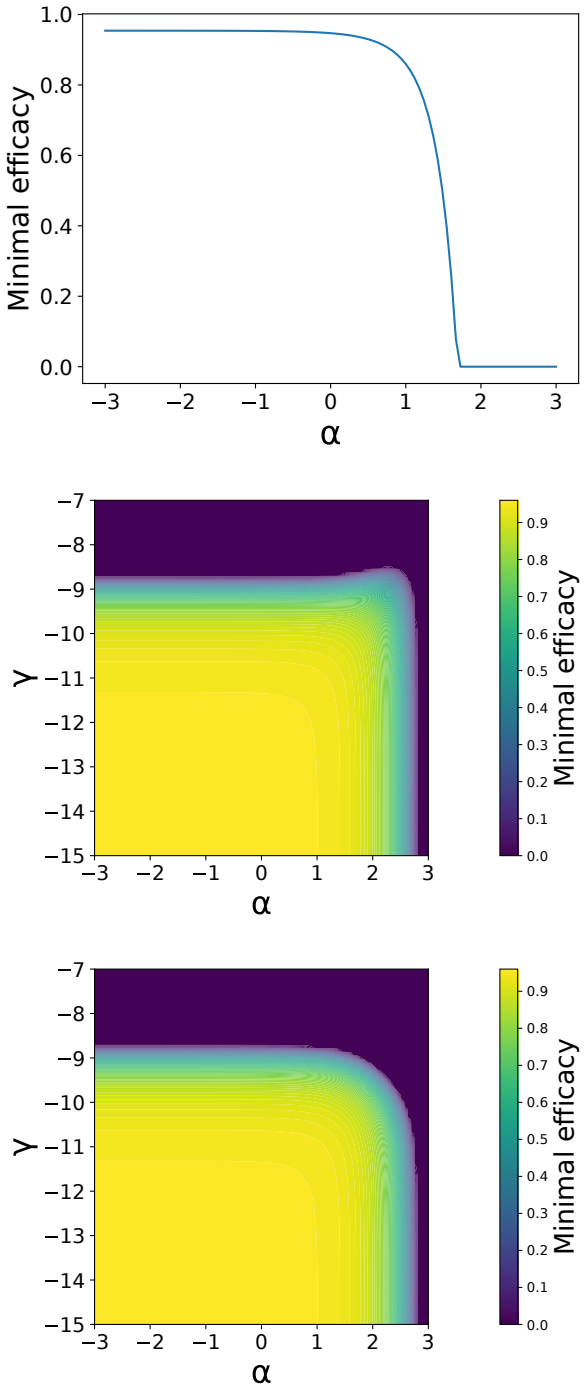

Figure 6. Minimal Drug efficacy required to send infection into decline for different models as a function of varied density dependent parameters. Minimal efficacy for varied density dependence Saturated Incidence (top), Beddington De-Angelis (middle), and Crowley-Martin (bottom). Note that α and γ are plotted on a logarithmic scale.

Based on the R_0, the minimal drug efficacy needed to cure an infection can be found. We define the efficacy of a drug, ε, as the fractional reduction in a particular viral replication process. When modeling the effect of a drug, we multiply the affected parameter, typically β or p, by $(1-\varepsilon)$, where ε is a number between 0 and 1. This results in the R_0 value also being reduced by $(1-\varepsilon)$. Recall that when R_0 is below 1, the infection's growth experiences a decline [50]. As a result, the minimal efficacy of a drug is the effectiveness required to reduce the infection's R_0 below one and can be found by the following relationship,

$$\varepsilon = 1 - \frac{1}{R_0}.$$

The minimal drug efficacies needed to cure are shown as functions of density dependence in Figure 6. For the saturated incidence model, as values of α increase, the minimal effective dose of a drug to send the infection into remission declines, but only at high values of α. This indicates that a lower dose of a drug may be effective when a density dependent infection rate is considered. For the Beddington DeAngelis model, the minimal effective dose remains constant and high, regardless of the density dependence, until the threshold values of α and γ are reached, at which point the minimal effectiveness substantially decreases. This indicates that density dependence does not noticeably affect minimal efficacy until a threshold parameter value is reached where the necessary effectiveness rapidly decreases. For the Crowley-Martin model, a similar effect of reaching a threshold value that results in subsequent decline in minimal effective dose required to eliminate infection is observed for high density dependent values of γ and α.

3.4. Infecting time

Values of infecting time were also calculated in order to determine the time required for a virus that has been produced to leave a cell and infect another cell. This provides insight into the system by increasing our understanding of the effect of speed of viral spread. The steps for the calculations were followed from González-Parra et al. [47].

The virus is produced at a rate p and cells going from the uninfected state to the eclipse state as a result of newly produced virus is described by $\frac{dE}{dt} = \beta TV$. To find the infecting time (t_{inf}), the time between virus production and infection of an uninfected cell is determined, so the rate at which cells leave the eclipse phase for the infected phase is not considered. We assume that the viral clearance during this time is negligible, therefore,

$$\frac{dV}{dt} = p$$

and

$$\frac{dE}{dt} = \frac{\beta V T_0}{1+\alpha V}$$

for the saturated incidence model. By integrating both equations, we find

$$\begin{aligned} V(t) &= pt \\ \int_0^1 dE &= \int_0^{t_{\text{inf}}} \frac{\beta T_0 pt}{1+\alpha pt} dt \\ 1 &= \beta T_0 p \int_0^{t_{\text{inf}}} \left(\frac{1}{\alpha p} - \frac{1}{\alpha p(\alpha pt+1)} \right) dt \end{aligned}$$

$$\begin{aligned} 1 &= \beta T_0 \left(\frac{t_{\text{inf}}}{\alpha p} - \frac{1}{\alpha^2 p} \int_0^{t_{\text{inf}}} \frac{1}{\alpha p t + 1} dt \right) \\ 1 &= \frac{\beta T_0 (\alpha p t_{\text{inf}} - \ln |\alpha p t_{\text{inf}} + 1|)}{\alpha^2 p}. \end{aligned} \tag{3.1}$$

Following the same logic as above, the infecting time relationship for the Beddington DeAngelis model can be integrated from,

$$\frac{dV}{dt} = p$$

and

$$\frac{dE}{dt} = \frac{\beta T_0 V}{1 + \alpha V + \gamma T_0}.$$

Integrating gives the following

$$\begin{aligned} \int_0^1 dE &= \int_0^{t_{\text{inf}}} \frac{\beta T_0 p t}{1 + \alpha p t + \gamma T_0} dt \\ 1 &= \beta T_0 p \int_0^{t_{\text{inf}}} \left(\frac{1}{\alpha p} + \frac{-\gamma T_0 - 1}{\alpha p (\alpha p t + \gamma T_0 + 1)} \right) dt. \end{aligned}$$

Following long division and integration, the infecting time relationship becomes

$$1 = \frac{\beta T_0}{\alpha^2 p} \left(\alpha p t_{\text{inf}} + (\gamma T_0 + 1) \ln \left| \frac{1 + \gamma T_0}{\alpha p t_{\text{inf}} + \gamma T_0 + 1} \right| \right). \tag{3.2}$$

For the Crowley Martin model,

$$\begin{aligned} V &= pt \\ \int_0^1 dE &= \int_0^{t_{\text{inf}}} \frac{\beta T_0 p t}{(1 + \alpha p t)(\gamma T_0 + 1)} dt \\ 1 &= \frac{\beta T_0 p}{\gamma T_0 + 1} \int_0^{t_{\text{inf}}} \left(\frac{1}{\alpha p} - \frac{1}{\alpha p (\alpha p t + 1)} \right) dt \\ 1 &= \frac{\beta T_0}{\gamma T_0 + 1} \left(\frac{t_{\text{inf}}}{\alpha} - \frac{1}{\alpha^2 p} \int_0^{t_{\text{inf}}} \frac{1}{\alpha p t + 1} dt \right) \\ 1 &= \frac{\beta T_0}{\alpha^2 p (1 + \gamma T_0)} \left(\alpha p t_{\text{inf}} - \ln \left| \frac{1 + \gamma T_0}{(\alpha p t_{\text{inf}} + 1)(1 + \gamma T_0)} \right| \right). \end{aligned} \tag{3.3}$$

All three models result in transcendental equations that we numerically solve for further insight. For all three models, a greater density dependence was associated with longer infecting times (Figure 7), thus indicating that increased heterogeneity impedes the virus's predicted ability to infect other cells.

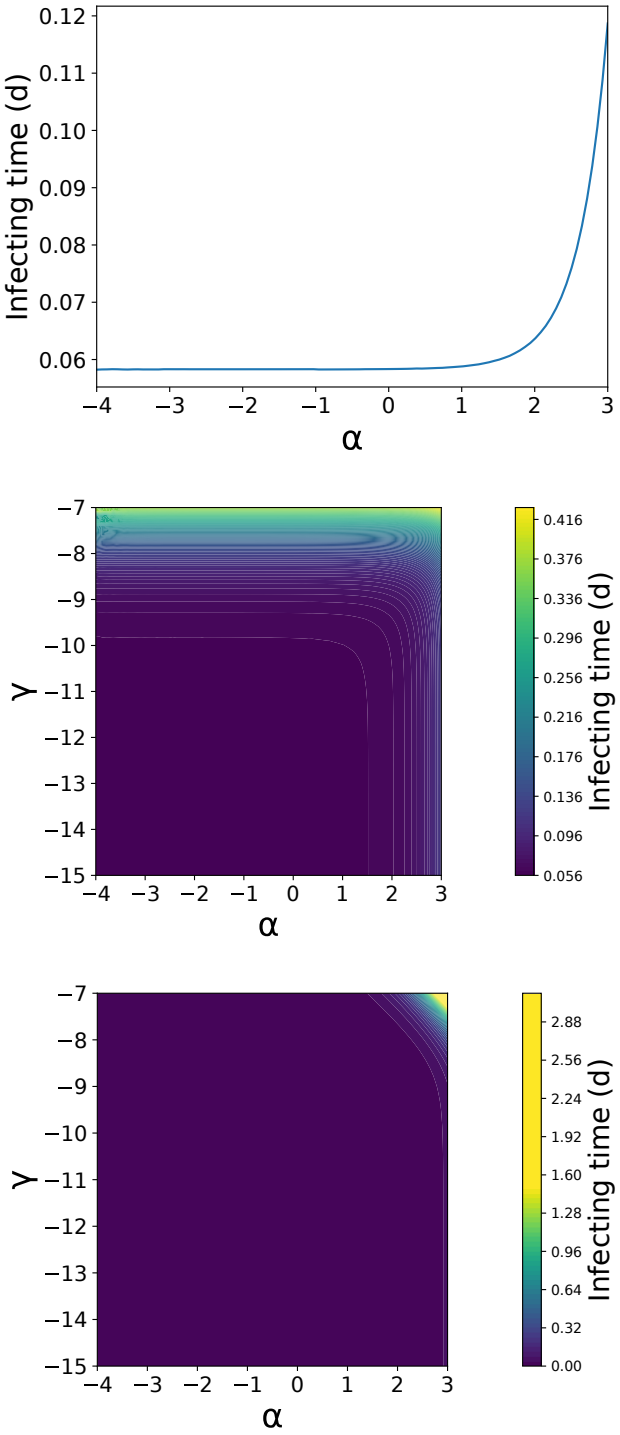

Figure 7. Infecting times for for varied density dependence. Saturated Incidence (top), Beddington De-Angelis (middle), and Crowley-Martin (bottom).

4. Discussion

We found that the incorporation of a density dependent infection rate alters the predicted progression of virus when compared to the basic viral kinetics model. The general trend for viral progression, as predicted by all three incidence functions, suggests a decrease in the infection severity as a result of density considerations. Specifically, increasing the density dependence of the infection rate leads to a lower viral upslope, alongside an earlier and lower viral titer peak. This slowing of infection progression is reflected in a lower basic reproduction number and a longer infecting time. The slowed initial progression of virus with a higher density dependence supports the notion that increased spatial heterogeneity in the initial stages of infection slows the infection as compared to a well-mixed system. Since the virus progresses by contact between uninfected target cells and viral particles, when virus particles have access to more uninfected target cells, the rate of infection progression is materially greater.

This finding has practical implications when using mathematical models for prediction. When using the basic infection model, we could be overestimating the growth rate of an infection and might even predict the growth of an infection when early spatial heterogeneity would actually drive the basic reproduction number below one, thus preventing growth of the infection. While we found that the density dependent infection rate has little effect on the minimum drug efficacy needed to cure an infection, density dependent infection could still alter the predicted viral decay rate when an antiviral treatment is implemented [51].

Experimental evidence supports spatial heterogeneity throughout influenza progression [52, 53]. A full account of spatial heterogeneity of viral spread can be done through the use of agent-based models (ABMs) [21, 53–58], which track each individual cell as it transitions from uninfected to infected to dead. However, these models are computationally expensive, which makes it difficult to model large numbers of cells in a reasonable time frame. Thus, the use of ordinary differential equations (ODEs), while less realistic than ABMs, is sometimes necessary to make predictions in a timely manner. Modifying ODEs in order to account for spatial heterogeneity allows us to take advantage of the computational speed of ODE models while potentially increasing the accuracy of the model predictions.

To date, a density dependent infection rate model has not been fit to experimental data. The basic model has been sufficient to capture the viral dynamics of all tested experimental data. This could be partly because of the limited number of data points collected in typical patient data, which often only has two points on the upslope [4], where the density dependent infection rate has the largest effect. Additionally, the fairly large measurement error of viral titer measurements [59] might make it difficult to detect subtle time course changes caused by a density dependent infection rate. However, in the work of Pinilla et al. [60], who simultaneously fitted a viral kinetics model to multiple cycle and single cycle assays, a roughly 12 h time shift was needed to fit the same model to both assays. It is interesting to note that the single cycle assay is spatially homogeneous since all cells are infected at the same time, while the multiple cycle assay, initiated with a low multiplicity of infection (MOI), is initially very spatially heterogeneous. A model that includes a density-dependent infection rate might be able to account for this difference. Additionally, the validity of the density dependent infection rate could be verified by fitting to viral time courses from ABMs. This would allow the direct determination of whether these functions can account for spatial heterogeneity, and can help to determine reasonable parameter ranges for α and γ.

Simulated viruses offer a window into how our biophysical understanding aligns with the predicted alteration in viral progression. Future work should include combining the density dependent infection

rate with models of other biological processes such as the adaptive and innate immune responses, coinfection, and drug resistance to improve fidelity of the models. All of these processes have the potential to be altered by the slower growing, milder infection predicted by density dependent infection rate models.

Author contributions

Conceptualization, HMD; Data curation, HS; Formal analysis, HS; Investigation, HS; Methodology, HS and HMD; Project administration, HMD; Software, HS; Supervision, HMD; Validation, HS and HMD; Visualization, HS; Writing – original draft, HS; Writing – review & editing, HMD.

Use of AI tools declaration

The authors declare they have not used Artificial Intelligence (AI) tools in the creation of this article.

Conflict of interest

The authors declare there is no conflict of interest.

References

1. M. A. Rolfes, I. M. Foppa, S. Garg, B. Flannery, L. Brammer, J. A. Singleton, et al., Annual estimates of the burden of seasonal influenza in the united states: A tool for strengthening influenza surveillance and preparedness, *Influenza Other Respir. Viruses*, **12** (2018), 132–137. https://doi.org/10.1111/irv.12486
2. *Centers for Disease Control and Prevention*, *Seasonal Flu Microsite*, 2022. Available from: https://www.cdc.gov/flu/season/2022-2023.html.
3. C. de Courville, S. M. Cadarette, E. Wissinger, F. P. Alvarez, The economic burden of influenza among adults aged 18 to 64: A systematic literature review, *Influenza Other Respir. Viruses*, **16** (2022), 376–385. https://doi.org/10.1111/irv.12963
4. P. Baccam, C. Beauchemin, C. A. Macken, F. G. Hayden, A. S. Perelson, Kinetics of influenza a virus infection in humans, *J. Virol.*, **80** (2006), 7590–7599. https://doi.org/10.1128/JVI.01623-05
5. G. González-Parra, H. M. Dobrovolny, Assessing uncertainty in A2 respiratory syncytial virus viral dynamics, *Comput. Math. Meth. Med.*, **2015** (2015), 567589. https://doi.org/10.1155/2015/567589
6. C. P. de Mello, X. Tao, T. H. Kim, M. Vicchiarelli, J. B. Bulitta, A. Kaushik, et al., Clinical regimens of favipiravir inhibit zika virus replication in the hollow-fiber infection model, *Antimicrob. Agents Chemother.*, **62** (2018), e00967–18. https://doi.org/10.1128/AAC.00967-18
7. E. A. Hernandez-Vargas, J. X. Velasco-Hernandez, In-host modelling of COVID-19 kinetics in humans, *Ann. Rev. Contr.*, **50** (2020), 448–456. https://doi.org/10.1101/2020.03.26.20044487
8. V. K. Nguyen, S. C. Binder, A. Boianelli, M. Meyer-Hermann, E. A. Hernandez-Vargas, Ebola virus infection modeling and identifiability problems, *Front. Microbiol.*, **6** (2015), 257. https://doi.org/10.3389/fmicb.2015.00257

9. C. Zitzmann, C. Daechert, B. Schmid, H. Van der Schaar, M. van Hemert, A. S. Perelson, et al., Mathematical modeling of plus-strand RNA virus replication to identify broad-spectrum antiviral treatment strategies, *PLoS Comput. Biol.*, **19** (2023), e1010423. https://doi.org/10.1371/journal.pcbi.1010423
10. K. Melville, T. Rodriguez, H. M. Dobrovolny, Investigating different mechanisms of action in combination therapy for influenza, *Front. Pharmacol.*, **9** (2018), 1207. https://doi.org/10.3389/fphar.2018.01207
11. C. A. Beauchemin, J. J. McSharry, G. L. Drusano, J. T. Nguyen, G. T. Went, R. M. Ribeiro, et al., Modeling amantadine treatment of influenza A virus *in vitro*, *J. Theor. Biol.*, **254** (2008), 439–451. https://doi.org/10.1016/j.jtbi.2008.05.031
12. C. A. A. Beauchemin, A. Handel, A review of mathematical models of influenza a infections within a host or cell culture: Lessons learned and challenges ahead, *BMC Public Health*, **11** (2011), S7. https://doi.org/10.1186/1471-2458-11-S1-S7
13. H. M. Dobrovolny, M. B. Reddy, M. A. Kamal, C. R. Rayner, C. A. Beauchemin, Assessing mathematical models of influenza infections using features of the immune response, *PLoS One*, **8** (2013), e57088. https://doi.org/10.1371/journal.pone.0057088
14. C. Zitzmann, L. Kaderali, Mathematical analysis of viral replication dynamics and antiviral treatment strategies: From basic models to age-based multi-scale modeling, *Front. Microbiol.*, **9** (2018), 1546. https://doi.org/doi:10.3389/fmicb.2018.01546
15. E. A. Hernandez-Vargas, E. Wilk, L. Canini, F. R. Toapanta, S. C. Binder, A. Uvarovskii, et al., Effects of aging on influenza virus infection dynamics, *J. Virol.*, **88** (2014), 4123–4131. https://doi.org/10.1128/JVI.03644-13
16. L. Canini, A. S. Perelson, Viral kinetic modeling: State of the art, *J. Theor. Biol.*, **242** (2006), 464–477. https://doi.org/10.1016/j.jtbi.2006.03.014
17. B. Fain, H. M. Dobrovolny, Initial inoculum and the severity of COVID-19: A mathematical modeling study of the dose-response of SARS-CoV-2 infections, *Epidemiologia*, **1** (2020), 5–15. https://doi.org/10.3390/epidemiologia1010003
18. D. S. Quan, Y. Weiming, Mathematical modeling of interaction between innate and adaptive immune responses in COVID-19 and implications for viral pathogenesis, *J. Med. Virol.*, **92** (2020), 1615–1628. https://doi.org/10.1002/jmv.25866
19. B. P. Holder, C. A. Beauchemin, Exploring the effect of biological delays in kinetic models of influenza within a host or cell culture, *BMC Public Health*, **11** (2011), S10. https://doi.org/10.1186/1471-2458-11-S1-S10
20. Y. Kakizoe, S. Nakaoka, C. A. Beauchemin, S. Morita, H. Mori, T. Igarashi, et al., A method to determine the duration of the eclipse phase for in vitro infection with a highly pathogenic SHIV strain, *Sci. Rep.*, **5** (2015), 10371. https://doi.org/10.1038/srep10371
21. B. Fain, H. M. Dobrovolny, GPU acceleration and data fitting: Agent-based models of viral infections can now be parameterized in hours, *J. Comput. Sci.*, **61** (2022), 101662. https://doi.org/10.1016/j.jocs.2022.101662

22. T. J. Sego, E. D. Mochan, G. B. Ermentrout, J. A. Glazier, A multiscale multicellular spatiotemporal model of local influenza infection and immune response, *J. Theor. Biol.*, **532** (2022), 110918. https://doi.org/10.1016/j.jtbi.2021.110918

23. B. P. Holder, L. E. Liao, P. Simon, G. Boivin, C. A. A. Beauchemin, Design considerations in building in silico equivalents of common experimental influenza virus assays and the benefits of such an approach, *Autoimmunity*, **44** (2011), 282–293. https://doi.org/10.3109/08916934.2011.523267

24. M. Keeling, The effects of local spatial structure on epidemiological invasions, *Proc. R. Soc. B Biol. Sci.*, **266** (1999), 859–867. https://doi.org/10.1098/rspb.1999.0716

25. S. H. Paull, S. Song, K. M. McClure, L. C. Sackett, A. M. Kilpatrick, P. T. J. Johnson, From superspreaders to disease hotspots: linking transmission across hosts and space, *Front. Ecol. Environ.*, **10** (2012), 75–82. https://doi.org/10.1890/110111

26. E. S. Nightingale, O. J. Brady, L. Yakob, C. C. W. Grp, The importance of saturating density dependence for population-level predictions of SARS-CoV-2 resurgence compared with density-independent or linearly density-dependent models, England, 23 March to 31 July 2020, *Eurosurveillance*, **26** (2021), 2001809. https://doi.org/10.2807/1560-7917.ES.2021.26.49.2001809

27. M. Hochberg, Nonlinear transmission rates and the dynamics of infectious disease, *J. Theor. Biol.*, **153** (1991), 301–321. https://doi.org/10.1016/S0022-5193(05)80572-7

28. H. Laarabi, E. H. Labriji, M. Rachik, A. Kaddar, Optimal control of an epidemic model with a saturated incidence rate, *Nonlinear Anal. Model. Control*, **17** (2012), 448–459. https://doi.org/10.15388/NA.17.4.14050

29. A. Kumar, Dynamic behavior of an SIR epidemic model along with time delay; Crowley-Martin type incidence rate and Holling type II treatment rate, *Int. J. Nonlinear Sci. Numer. Simul.*, **20** (2019), 757–771. https://doi.org/10.1515/ijnsns-2018-0208

30. X. Wang, Y. Tao, X. Song, A delayed HIV-1 infection model with Beddington-DeAngelis functional response, *Nonlinear Dyn.*, **62** (2010), 67–72. https://doi.org/10.1007/s11071-010-9699-1

31. K. Hattaf, N. Yousfi, A. Tridane, Mathematical analysis of a virus dynamics model with general incidence rate and cure rate, *Nonlinear Anal. Real World Appl.*, **13** (2012), 1866–1872. https://doi.org/10.1016/j.nonrwa.2011.12.015

32. M. K. Singh, A. Anjali, B. K. Singh, C. Cattani, Impact of general incidence function on three-strain SEIAR model, *Math. Biosci. Eng.*, **20** (2023), 19710–19731. https://doi.org/10.3934/mbe.2023873

33. H. Hethcote, P. Vandendriessche, Some epidemiologic models with nonlinear incidence, *J. Math. Biol.*, **29** (1991), 271–287. https://doi.org/10.1007/BF00160539

34. G. Huang, Y. Takeuchi, W. Ma, D. Wei, Global stability for delay SIR and SEIR epidemic models with nonlinear incidence rate, *Bull. Math. Biol.*, **72** (2010), 1192–1207. https://doi.org/10.1007/s11538-009-9487-6

35. A. P. Smith, D. J. Moquin, V. Bernhauerova, A. M. Smith, Influenza virus infection model with density dependence supports biphasic viral decay, *Front. Microbiol.*, **9** (2018), 1554. https://doi.org/10.3389/fmicb.2018.01554

36. A. Gerg, H. M. Dobrovolny, Quantifying impact of HIV receptor surface density reveals differences in fusion dynamics of HIV strains, *Viruses*, **17** (2025), 583. https://doi.org/10.3390/v17040583

37. A. Farrell, T. Phan, C. B. Brooke, K. Koelle, R. Ke, Semi-infectious particles contribute substantially to influenza virus within-host dynamics when infection is dominated by spatial structure, *Virus Evol.*, **9** (2023), vead020. https://doi.org/10.1093/ve/vead020

38. A. M. Elaiw, S. A. Azoz, Global properties of a class of HIV infection models with beddington-deangelis functional response, *Math. Method Appl. Sci.*, **36** (2013), 383–394. https://doi.org/10.1002/mma.2596

39. G. Huang, W. Ma, Y. Takeuchi, Global analysis for delay virus dynamics model with beddington–deangelis functional response, *Appl. Math. Lett.*, **24** (2011), 1199–1203. https://doi.org/https://doi.org/10.1016/j.aml.2011.02.007

40. Z. T. H. Miao, X. Abdurahman, Stability and hopf bifurcation for a five-dimensional virus infection model with beddington–deangelis incidence and three delays, *J. Biol. Dyn.*, **12** (2018), 146–170. https://doi.org/10.1080/17513758.2017.1408861

41. G. Huang, W. Ma, Y. Takeuchi, Global properties for virus dynamics model with beddington–deangelis functional response, *Appl. Math. Lett.*, **22** (2009), 1690–1693. https://doi.org/https://doi.org/10.1016/j.aml.2009.06.004

42. H. Hu, K. Nigmatulina, P. Eckhoff, The scaling of contact rates with population density for the infectious disease models, *Math. Biosci.*, **244** (2013), 125–134. https://doi.org/10.1016/j.mbs.2013.04.013

43. J. Tripathi, S. Bugalia, V. Tiwari, Y. Kang, A predator–prey model with crowley–martin functional response: a nonautonomous study, *Nat. Resour. Model.*, **33** (2020), e12287. https://doi.org/10.1111/nrm.12287

44. N. Kumar, Dynamic behavior of an SIR epidemic model along with time delay; crowley-martin type incidence rate and holling type II treatment rate, *Int. J. Nonlinear Sci. Num.*, **20** (2019), 757–771. https://doi.org/10.1515/ijnsns-2018-0208

45. O. Diekmann, J. A. P. Heesterbeek, M. G. Roberts, The construction of next-generation matrices for compartmental epidemic models, *J. R. Soc. Interface*, **7** (2010), 873–885. https://doi.org/10.1098/rsif.2009.0386

46. H. M. Dobrovolny, R. Gieschke, B. E. Davies, N. L. Jumbe, C. A. A. Beauchemin, Neuraminidase inhibitors for treatment of human and avian strain influenza: A comparative study, *J. Theor. Biol.*, **269** (2011), 234–244. https://doi.org/10.1016/j.jtbi.2010.10.017

47. G. González-Parra, F. De Ridder, D. Huntjens, D. Roymans, G. Ispas, H. M. Dobrovolny, A comparison of RSV and influenza *in vitro* kinetic parameters reveals differences in infecting time, *PLoS One*, **13** (2018), e0192645. https://doi.org/10.1371/journal.pone.0192645

48. L. Pinky, H. M. Dobrovolny, The impact of cell regeneration on the dynamics of viral coinfection, *Chaos*, **27** (2017), 063109. https://doi.org/10.1063/1.4985276

49. A. M. Smith, F. R. Adler, A. S. Perelson, An accurate two-phase approximate solution to an acute viral infection model, *J. Math. Biol.*, **60** (2010), 711–726. https://doi.org/10.1007/s00285-009-0281-8

50. N. F. Beggs, H. M. Dobrovolny, Determining drug efficacy parameters for mathematical models of influenza, *J. Biol. Dyn.*, **9** (2015), 332–346. https://doi.org/10.1080/17513758.2015.1052764

51. J. Palmer, H. M. Dobrovolny, C. A. Beauchemin, The *in vivo* efficacy of neuraminidase inhibitors cannot be determined from the decay rates of influenza viral titers observed in treated patients, *Sci. Rep.*, **7** (2017), 40210. https://doi.org/10.1038/srep40210

52. M. E. Gallagher, C. B. Brooke, R. Ke, K. Koelle, Causes and consequences of spatial within-host viral spread, *Viruses*, **10** (2018), 627. https://doi.org/10.3390/v10110627

53. C. Beauchemin, Probing the effects of the well-mixed assumption on viral infection dynamics, *J. Theor. Biol.*, **242** (2006), 464–477. https://doi.org/10.1016/j.jtbi.2006.03.014

54. D. Wodarz, C. N. Chan, B. Trinite, N. L. Komarova, D. N. Levy, On the laws of virus spread through cell populations, *J. Virol.*, **88** (2014), 13240–13248. https://doi.org/10.1128/JVI.02096-14.

55. X. Tong, J. Chen, H. Miao, T. Li, L. Zhang, Development of an agent-based model (ABM) to simulate the immune system and integration of a regression method to estimate the key ABM parameters by fitting the experimental data, *PLoS One*, **10** (2015), e0141295. https://doi.org/10.1371/journal.pone.0141295

56. J. Whitman, A. Dhanji, F. Hayot, S. C. Sealfon, C. Jayaprakash, Spatio-temporal dynamics of host-virus competition: A model study of influenza A, *J. Theor. Biol.*, **484** (2020), 110026. https://doi.org/10.1016/j.jtbi.2019.110026

57. A. Goyal, J. M. Murray, Modelling the impact of cell-to-cell transmission in hepatitis B virus, *PLoS One*, **11** (2016), e0161978. https://doi.org/10.1371/journal.pone.0161978

58. S. Wasik, P. Jackowiak, M. Figlerowicz, J. Blazewicz, Multi-agent model of hepatitis C virus infection, *Artif. Intell. Med.*, **60** (2014), 123–131. https://doi.org/10.1016/j.artmed.2013.11.001

59. D. LaBarre, R. Lowy, Improvements in methods for calculating virus titer estimates from $TCID_{50}$ and plaque assays, *J. Virol. Meth.*, **96** (2001), 107–126. https://doi.org/10.1016/S0166-0934(01)00316-0

60. L. T. Pinilla, B. P. Holder, Y. Abed, G. Boivin, C. A. A. Beauchemin, The H275Y neuraminidase mutation of the pandemic A/H1N1 influenza virus lengthens the eclipse phase and reduces viral output of infected cells, potentially compromising fitness in ferrets, *J. Virol.*, **86** (2012), 10651–10660. https://doi.org/10.1128/JVI.07244-11

AIMS Press

© 2026 the Author(s), licensee AIMS Press. This is an open access article distributed under the terms of the Creative Commons Attribution License (http://creativecommons.org/licenses/by/4.0)